ELSEVIER

Journal of Fluids and Structures 21 (2005) 543–559

JOURNAL OF FLUIDS AND STRUCTURES

www.elsevier.com/locate/jfs

Enhanced nonlinear dynamics and monitoring bifurcation morphing for the identification of parameter variations

S.-H. Yin, B.I. Epureanu*

Department of Mechanical Engineering, University of Michigan, 2350 Hayward Street, Ann Arbor, MI 48109-2125, USA

Received 25 May 2005; accepted 27 July 2005
Available online 27 October 2005

Abstract

This paper proposes a novel vibration-based damage detection approach. The proposed technique is to actively change the stability of a fixed point (equilibrium state) of a system (structure) and create a new stable fixed point or limit cycle by applying a nonlinear feedback excitation. The nonlinear feedback excitation is designed such that a desired bifurcation (e.g., subcritical Hopf bifurcation) can occur, and a limit cycle may emerge close to the original fixed point. Hence, the deterioration of the structure during measurements is prevented, while the sensitivity of detection is increased by identifying the bifurcation point. The morphing of the bifurcation boundary (the locus of the bifurcation points) in the space of the controlled parameters of the nonlinear feedback excitation, together with the difference in the amplitude of the emerging limit cycle caused by the variation in structural parameters are utilized as features for the identification of parameter variations. To demonstrate the applicability and the potential (high sensitivity and robustness) offered by the proposed approach, a prototypical case of a two-degree-of-freedom mass–spring–damper system and a more complex example of a nonlinear panel forced by aerodynamic loads are investigated.

Keywords: Damage detection; Nonlinear feedback excitation; Bifurcations

1. Introduction

Vibration-based techniques are commonly used for the identification of parameter variations in applications such as nondestructive evaluation and damage detection (Doebling et al., 1996; Farrar et al., 2001). Such detection methods monitor changes in various vibratory characteristics of a structure. For instance, most current vibration-based damage detection techniques observe changes in natural frequencies, modes of vibration, and frequency response functions (Loh and Tou, 1995; Doebling et al., 1996; Smyth et al., 2000; Farrar et al., 2001). Other techniques use subspace identification and updating (Abdalla et al., 1998; Pappa et al., 1998; Zimmerman, 2000; D'Souza and Epureanu, 2005a, b), wavelet analyses (Sohn and Farrar, 2001; Amizic et al., 2002; Amaravadi et al., 2002), and Ritz vectors (Cao and Zimmerman, 1999; Zimmerman, 1999). All these methods have been well developed for monitoring linear structures. Although there have been numerous studies showing that changes in these linear observed features can be used to detect parameter variations indicative of the presence of damage, the low sensitivity of these features (to damage) limits the applicability of such methods to cases where very precise measurements are available, or high levels

*Corresponding author. Tel.: +1 734 647 6391; fax: +1 734 615 6647.
E-mail address: epureanu@umich.edu (B.I. Epureanu).

0889-9746/$ - see front matter © 2005 Elsevier Ltd. All rights reserved.
doi:10.1016/j.jfluidstructs.2005.07.017

of damage are to be detected. To increase sensitivity to parameter variations, the concept of sensitivity enhanced control was proposed through linear feedback control applied to a structure (Ray and Tian, 1999; Ray and Koh, 2003; Koh and Ray, 2003). Such an approach reduces the modal frequencies to enhance their sensitivity to changes in stiffness.

One of the reasons for the limitations of current methods is that they are designed to avoid as much as possible the influence of nonlinearities. In contrast, several other approaches to identify damage exploit attractor-based features derived from nonlinear time series of the dynamics. Some attractors (such as limit cycles) have been used, but they are not very sensitive, which makes it difficult to detect small incipient damage (Epureanu et al., 2004a, b). To enhance sensitivity, nonlinearities have been exploited by characterizing chaotic attractors. For example, linear systems subjected to chaotic excitation (Nichols et al., 2003a–d; Trickey et al., 2002) and (nonlinear) chaotic systems (with or without excitation) (Epureanu and Yin, 2004; Epureanu et al., 2004b, c) have been explored to show that the use of nonlinearity holds a great potential for damage detection. Furthermore, enhancing nonlinearity of linear or weakly nonlinear systems by means of nonlinear feedback excitation has been demonstrated to provide significant advantages, such as increased sensitivity (Epureanu et al., 2005a, b). Also, a variety of attractor-based metrics to characterize quantitatively the geometry of attractors in state–space have been presented for identifying changes in geometric features of attractors due to changes in system parameters (i.e., damage). Some of these methods use Lyapunov exponents or attractor dimensions (Chancellor et al., 1996; Wang et al., 2001), a scalar tracking metric (Chelidze et al., 2002; Cusumano et al., 2002; Chatterjee et al., 2002; Chelidze and Cusumano, 2004), and average local attractor variance ratios (Nichols et al., 2003b; Todd et al., 2001), while others employ the statistical characterization of the distribution of points in an attractor (Epureanu et al., 2004c, 2005a; Epureanu and Yin, 2004; Trendafilova, 2003a, b). Most such approaches may detect the presence of damage while only very few (Epureanu et al., 2004c, 2005a; Epureanu and Yin, 2004) are able to identify damage location and level. Most approaches have difficulties identifying multiple damage also (Chatterjee et al., 2002; Chelidze and Cusumano, 2004; Todd et al., 2001; Trendafilova, 2003a, b). To address these limitations, the application of pattern recognition techniques based on proper orthogonal decomposition of the shape changes between attractors for damaged systems and the healthy system may provide the basis for detecting multiple simultaneous damages (Epureanu and Yin, 2004).

In the present work, we proposed a distinct and novel damage detection method which is based on observing the onset of bifurcations and the dynamics in the post-bifurcation regime. Although based on nonlinear phenomena, this approach is very different from attractor-based techniques. The key idea of the proposed method is to actively change the stability of the original fixed point (equilibrium state) of a system (structure) and create a new stable fixed point or limit cycle by applying a nonlinear feedback excitation to the system (structure). As opposed to usual external excitations, the nonlinear feedback excitation requires the active measurement of the dynamics and a feedback loop. The specific form of the nonlinear feedback is designed based on the desired type of bifurcation. Hence, the proposed technique is an active system interrogation approach based on nonlinear feedback. A bifurcation point is designed (in a beneficial way) so that its location is sensitive to the variation in a desired parameter (e.g., damage). The actual bifurcation point can be determined by varying the value of the gains in the nonlinear feedback excitation and recording the value at which the bifurcation occurs. In the parameter space, the locus of the bifurcation points is in general a curve which characterizes a large number of bifurcation points exhibiting the same type of bifurcation. This curve provides a boundary separating the parameter space in regions where the dynamics is qualitatively distinct. In the proposed approach, the bifurcation boundary and the corresponding emerging dynamics are used as features to detect multiple simultaneous parameter variations (e.g., damages). Given a (measured) boundary for the damaged structure, multiple simultaneous damages can be detected by quantifying the displacement of the measured boundary with respect to the boundary for the healthy structure. Important advantages of the proposed approach are its possibility to be optimized for each application through the optimization of the nonlinear feedback excitation, as well as its robustness to measurement noise. To demonstrate the proposed approach, we consider first a prototypical case of a two-degree-of-freedom mass–spring–damper system, and then investigate a more complex example of a nonlinear panel forced by aerodynamic loads. The scenarios for the damage occurring in the structure are modelled as loss of stiffness of structural elements.

2. Methodology

2.1. Background explanation

For most structures, dissipative mechanisms balance the external excitation such that the dynamics evolves onto an invariant manifold of the state–space (the attractor). Examples of attractors of the dynamics of a structure are stable

fixed points, stable limit cycles, and strange attractors (for chaotic systems). A qualitative change in the dynamics (referred to as a *bifurcation*) may happen as parameters are varied. For example, fixed points or limit cycles can be destroyed or created, or their stability can change when bifurcations occur. In the present work, the proposed damage detection method is based on observing the onset of bifurcations and the emerging dynamics in the post-bifurcation regime. The controlled parameters (gains) of the nonlinear feedback excitation are manipulated to interrogate the system by identifying and characterizing bifurcation points.

To present this idea, an example based on a single-degree-of-freedom oscillator excited by a specific feedback is discussed next. A more detailed discussion is also included in the following sections. The governing equation for this system may be expressed as

$$\begin{bmatrix} \dot{x} \\ \ddot{x} \end{bmatrix} = \begin{bmatrix} 0 & 1 \\ -k/m & -c/m \end{bmatrix} \begin{bmatrix} x \\ \dot{x} \end{bmatrix} + \begin{bmatrix} 0 \\ 1/m \end{bmatrix} \left[ax - \beta x^3\right], \tag{1}$$

where m, c, and k are mass, damping, and stiffness parameters, a and β are the linear and nonlinear gains, while the state vector is composed of the position x and the velocity $\dot{x}$. All of parameters are assumed to be positive. An eigenvalue analysis of the Jacobian matrix shows that the origin in state–space ($x = 0$, $\dot{x} = 0$) is a stable fixed point as long as the linear gain a is less than k. When a reaches k, a supercritical pitchfork bifurcation occurs as shown in Fig. 1. Hence, the fixed point at the origin loses stability, and two new stable fixed points appear at states $(\pm\sqrt{(a-k)/\beta}, 0)$. Thus, the stiffness k may be directly interrogated by varying the value of the linear gain a to observe the onset of bifurcation in this special case. Therefore, the change in stiffness due to damage can be detected by distinguishing between the bifurcation point for a healthy and a damaged system. One may notice that the linear feedback ax is designed to destabilize the system, and the nonlinear feedback $-\beta x^3$ is designed to limit the system displacement in the post-bifurcation regime. Also, the type of bifurcation and the dynamics in the post-bifurcation regime depend on the form of the nonlinear feedback and the nonlinear gain. For example, if a different kind of nonlinear feedback (such as $\beta x^3 - \gamma x^5$) is used to replace $-\beta x^3$ in Eq. (1), then a different type of bifurcation (a subcritical pitchfork bifurcation) may occur when a is equal to k as shown in Fig. 1. In the case of a subcritical pitchfork bifurcation, the jump in displacement for the system at the bifurcation point ($a = k$) can be detected, and it is equal to $\sqrt{\beta/\gamma}$. From the viewpoint of interrogating for k, this jump can facilitate to identify the bifurcation point more precisely. However, a jump that is too large may break the system. Thus, the nonlinear gains β and γ are designed such that the jump at $a = k$ is as small as possible while maintaining high enough sensitivity.

This simple example was presented to introduce the basic idea of the proposed damage detection technique. Also, some important issues regarding the design of the nonlinear feedback excitation used in this technique have been addressed. The details of the methodology are presented in the next section.

2.2. Damage detection technique

To apply this idea for damage detection to a more realistic and complex structure, consider first that a discretized model of the structure (e.g., based on a finite element or a finite difference formulation) is available. The equation of motion for the discretized structural model can be expressed as

$$\mathbf{M}\ddot{\mathbf{x}} + \mathbf{C}\dot{\mathbf{x}} + \mathbf{K}\mathbf{x} = \mathbf{F}, \tag{2}$$

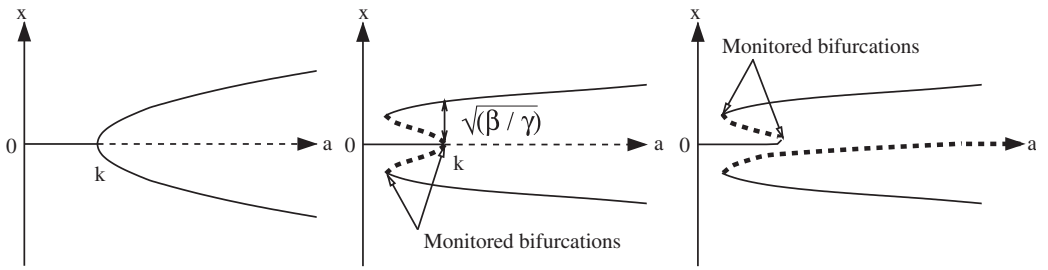

Fig. 1. Schematic plot of the equilibrium location of a single-degree-of-freedom oscillator forced by nonlinear feedback excitation undergoing a supercritical (left) and subcritical (symmetric: center, and imperfect: right) pitchfork bifurcation.

where matrices **M**, **C**, and **K** are mass, damping, and stiffness matrices, and **x** is the vector of nodal displacements. By introducing a new vector $\mathbf{v} = \dot{\mathbf{x}}$, Eq. (2) can be expressed in state–space representation as

$$\dot{\mathbf{X}} = \mathbf{A}\mathbf{X} + \mathbf{B}\mathbf{F}, \tag{3}$$

where

$$\mathbf{X} = [\mathbf{x}\ \ \mathbf{v}]^{\mathrm{T}},$$

$$\mathbf{F} = \mathbf{G}\mathbf{X} + \bar{\mathbf{F}}(\mathbf{X}),$$

$$\mathbf{A} = \begin{bmatrix} \mathbf{0} & \mathbf{I} \\ -\mathbf{M}^{-1}\mathbf{K} & -\mathbf{M}^{-1}\mathbf{C} \end{bmatrix}, \quad \mathbf{B} = \begin{bmatrix} \mathbf{0} \\ \mathbf{M}^{-1} \end{bmatrix}.$$

Herein, the nonlinear feedback excitation **F** is a function of **x** and $\dot{\mathbf{x}}$, and consists of linear feedback **GX** and nonlinear feedback $\bar{\mathbf{F}}(\mathbf{X})$, where **G** denotes the linear gain matrix.

Generally, for most autonomous systems, the origin in the state–space is a stable fixed point (equilibrium state) to which the dynamics converges. The key idea of the proposed method is to actively change the stability of the fixed point at the origin by tuning the values of the entries in the gain matrix **G**, and to design the nonlinear feedback $\bar{\mathbf{F}}(\mathbf{X})$ such that a new stable fixed point or a limit cycle can emerge close to the origin. For simplicity, the bifurcation caused by the designed nonlinear feedback excitation is chosen to be a co-dimension one bifurcation, which includes two cases. One case is where one of the real eigenvalues of the Jacobian matrix at the origin passes through the imaginary axis from left to right. The other case is where one pair of complex conjugate eigenvalues cross the imaginary axis from left to right. It is well known that the former is related to a pitchfork bifurcation and the latter is associated with a Hopf bifurcation. In the proposed approach, the changes in the locus of bifurcation points in the parameter space are exploited to identify the changes in structural parameters caused by damage. Whether numerically simulating or experimentally implementing this approach, the locus of bifurcation points can be obtained by varying the values of the controlled parameters in the gain matrix **G** and recording the specific values at which a pitchfork or Hopf bifurcation occurs. Hence, a boundary separating the parameter space in regions where the dynamics is qualitatively distinct is identified.

Mathematically, the analytical equation characterizing the bifurcation boundary can be obtained by exploring the eigenvalues of the Jacobian matrix at the origin. For the dynamics of the structure governed by Eq. (3), the Jacobian matrix at the origin can be expressed as $\mathbf{A} + \mathbf{B}\mathbf{G}$, and its characteristics polynomial can be obtained as

$$|\mathbf{A} + \mathbf{B}\mathbf{G} - \lambda\mathbf{I}| = 0. \tag{4}$$

The exact equation describing the pitchfork bifurcation boundary can be obtained by substituting $\lambda = 0$ into Eq. (4). For the Hopf bifurcation boundary, λ is substituted with $\pm\omega\mathrm{j}$ into Eq. (4) (where $\mathrm{j} = \sqrt{-1}$, and ω is real and positive). The resulting equations (corresponding to the real and imaginary parts) need to be solved simultaneously to obtain the exact boundary equation. Also, one may note that Eq. (4) is independent of the nonlinear feedback, which means that the determination of bifurcation points on the boundary is not affected by the nonlinear feedback. However, the nonlinear feedback can play an important role in the post-bifurcation behavior of the system, such as determining the subcritical or supercritical nature of the bifurcation. Based on the analytical solution for the bifurcation boundary, the relationship between system parameters and bifurcation points can be clearly demonstrated, and explains why the parametric variations in the system can be interrogated by monitoring the morphing of the bifurcation boundary.

To address these issues, a damped two-degree-of-freedom spring–mass system shown in Fig. 2 is considered. The mass, damping, and stiffness matrices (**M**, **C**, and **K**) in the equation of motion of this system are expressed as

$$\mathbf{M} = \begin{bmatrix} m_1 & 0 \\ 0 & m_2 \end{bmatrix}, \quad \mathbf{C} = \begin{bmatrix} c_1 + c_2 & -c_2 \\ -c_2 & c_2 \end{bmatrix}, \quad \mathbf{K} = \begin{bmatrix} k_1 + k_2 & -k_2 \\ -k_2 & k_2 \end{bmatrix}.$$

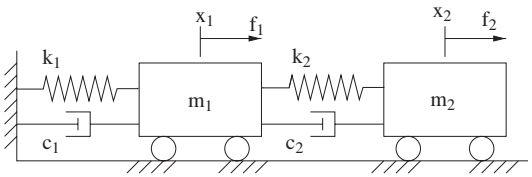

Fig. 2. A simple two-degree-of-freedom system subjected to nonlinear feedback excitation.

The goal of the design of the linear feedback **GX** is to change the stability of the fixed point at the origin. To achieve this objective, an intuitive way is to decrease the stiffness of the system as demonstrated in a simple example in Section 2.1. Therefore, the entries in the gain matrix **G** corresponding to x_1 and x_2 are chosen to be the controlled parameters. For simplicity, in this study, only two entries are considered variable while the others are considered fixed. As a result, the bifurcation boundary is a curve in the parameter space spanned by the two controlled variable parameters. Also, a single excitation is considered to be applied to the systems in the following examples. Herein, the feedback excitation is designed as

$$\begin{aligned}\mathbf{F} &= \mathbf{GX} + \bar{\mathbf{F}}(\mathbf{X}) \\ &= \begin{bmatrix} 0 & 0 & 0 & 0 \\ a & b & 0 & 0 \end{bmatrix} \begin{bmatrix} x_1 \\ x_2 \\ \dot{x}_1 \\ \dot{x}_2 \end{bmatrix} + \begin{bmatrix} 0 \\ f(x_1, x_2) \end{bmatrix} = \begin{bmatrix} 0 \\ ax_1 + bx_2 + f(x_1, x_2) \end{bmatrix},\end{aligned} \tag{5}$$

where the nonlinear feedback $f(x_1, x_2)$ is discussed in detail in the next section. Furthermore, the governing equation for this system can be expressed in the state–space form of Eq. (3) with

$$\mathbf{A} = \begin{bmatrix} 0 & 0 & 1 & 0 \\ 0 & 0 & 0 & 1 \\ -(k_1 + k_2)/m_1 & k_2/m_1 & -(c_1 + c_2)/m_1 & c_2/m_1 \\ k_2/m_2 & -k_2/m_2 & c_2/m_2 & -c_2/m_2 \end{bmatrix},$$

$$\mathbf{B} = \begin{bmatrix} 0 & 0 \\ 0 & 0 \\ 1/m_1 & 0 \\ 0 & 1/m_2 \end{bmatrix}, \quad \mathbf{X} = \begin{bmatrix} x_1 \\ x_2 \\ \dot{x}_1 \\ \dot{x}_2 \end{bmatrix}.$$

Thus, the Jacobian matrix at the origin can be obtained as

$$\mathbf{A} + \mathbf{BG} = \begin{bmatrix} 0 & 0 & 1 & 0 \\ 0 & 0 & 0 & 1 \\ -(k_1 + k_2)/m_1 & k_2/m_1 & -(c_1 + c_2)/m_1 & c_2/m_1 \\ (a + k_2)/m_2 & (b - k_2)/m_2 & c_2/m_2 & -c_2/m_2 \end{bmatrix}.$$

Based on Eq. (4), one may specify the conditions for pitchfork or Hopf bifurcations ($\lambda = 0$ or $\lambda = \pm\omega \mathrm{j}$). Then, the exact equations describing the pitchfork and the Hopf bifurcation boundaries can be obtained as

$$\begin{vmatrix} -(k_1 + k_2)/m_1 & k_2/m_1 \\ (a + k_2)/m_2 & (b - k_2)/m_2 \end{vmatrix} = 0 \tag{6}$$

and

$$\phi^2 - \frac{[m_1 b - m_2 k_1 - (m_1 + m_2)k_2 - c_1 c_2]}{m_1 m_2}\phi - \frac{[k_2 a + (k_1 + k_2)b - k_1 k_2]}{m_1 m_2} = 0, \tag{7}$$

where

$$\phi = \frac{[c_2 a + (c_1 + c_2)b - k_1 c_2 - k_2 c_1]}{m_1 c_2 + m_2 c_1 + m_2 c_2}.$$

Eqs. (6) and (7) clearly show that the bifurcation boundaries are dependent on the system parameters. Thus, parametric variations will cause geometric changes of the bifurcation boundaries. To demonstrate quantitatively the morphing of the bifurcation boundaries, we choose the system parameters of the healthy system as $m_1 = m_2 = 1$, $k_1 = k_2 = 1$, $c_1 = c_2 = 1$, while loss of spring stiffness is modelled as damage. For example, $k_1 = 0.9$ or $k_2 = 0.8$ represent different levels of damage occurring at different locations. Fig. 3 shows that pitchfork and Hopf bifurcation loci provide boundaries separating the parameter space into three regions. When the parameters (a, b) in the linear gain matrix **G** are within the lower center region, the origin is a stable fixed point. If the parameters (a, b) cross the Hopf

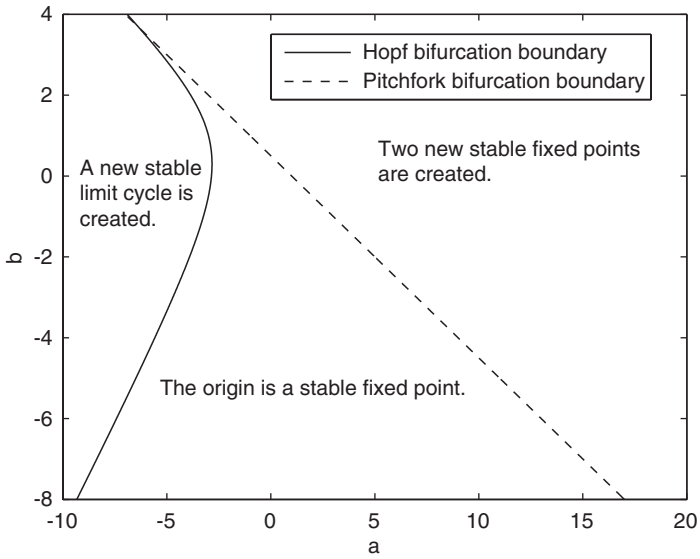

Fig. 3. Loci for the pitchfork and Hopf bifurcations in the parameter space (a, b) for a two-degree-of-freedom spring–mass–damper system subjected to a nonlinear feedback excitation, where a and b are controlled parameters in the linear gain matrix $\mathbf{G}$.

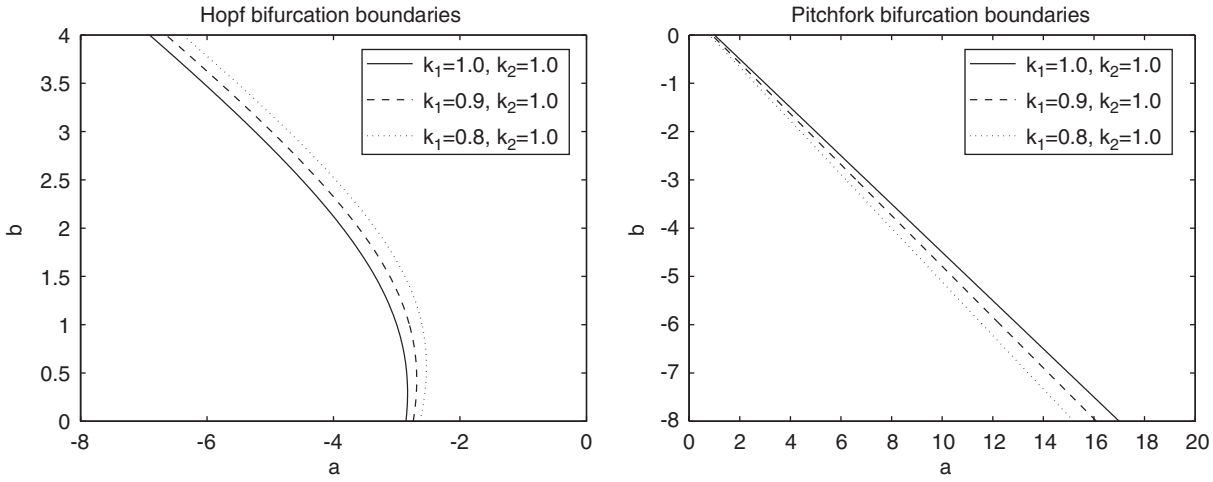

Fig. 4. Hopf and pitchfork bifurcation boundaries for the healthy system and damaged systems where different parametric variations in k_1 are used to model different levels of damage.

bifurcation boundary and enter the left region, the fixed point at the origin loses its stability and a new stable limit cycle is created close to the origin. In contrast, if the parameters (a, b) cross the pitchfork bifurcation boundary and enter the right region, the fixed point at the origin also becomes unstable and two new stable fixed points are born near the origin. Fig. 4 shows that the Hopf and pitchfork bifurcation boundaries move and deform when the parameter k_1 varies (due to damage). In this figure, one may note that the bifurcation locus in some regions of parameter space is more sensitive to the variation in parameters than other regions. This implies that the range of the controlled parameters used in the gain matrix $\mathbf{G}$ can be designed in a beneficial way so that the movement of the bifurcation boundary is sensitive to the variation in a desired parameter (damage). Also, we consider that the stiffnesses of the two springs in the system are changed singly or simultaneously to simulate different locations of damage and multiple damages. Fig. 5 shows that the Hopf and pitchfork bifurcation boundaries for different damage cases shift and deform in different ways with respect to

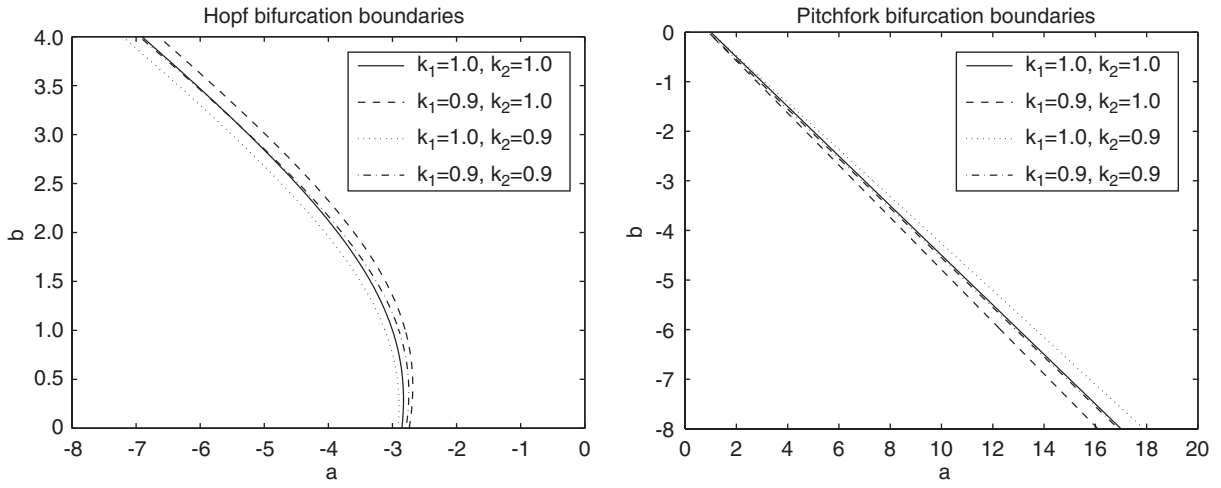

Fig. 5. Hopf and pitchfork bifurcation boundaries for the healthy system and damaged systems where parametric variations (singly or simultaneously in k_1 and k_2) are used to model different locations of damage and multiple damages.

the bifurcation boundaries (the solid curves) for the healthy system ($k_1 = k_2 = 1$). The morphing of these boundaries is essential for detecting damage location.

Also, *multiple simultaneous* damages may be detected by quantifying the displacement of the measured boundary with respect to the boundary for the healthy system. To explain this, the bifurcation boundary curve can be considered as a function of the identified parameters (k_1 and k_2) and the controlled parameters (a and b), and expressed as $a = g(b, k_1, k_2)$ for a given set of k_1 and k_2. We are interested in understanding the sensitivity of the movement of the curve to the variation in k_1 and k_2. Suppose there is no variation in parameter b and the variations in other parameters are small. The displacement Δa of the measured boundary (for the damaged system) with respect to the reference boundary (i.e., for the healthy system) can be written as

$$\Delta a = \frac{\partial g}{\partial k_1}\Delta k_1 + \frac{\partial g}{\partial k_2}\Delta k_2. \tag{8}$$

The variation in a due to the variation in k_1 and k_2 can be described by the sensitivity functions $\partial g/\partial k_1$ and $\partial g/\partial k_2$, which are functions of k_1, k_2, and b. The shapes of $\partial g/\partial k_1$ and $\partial g/\partial k_2$ can be visualized by fixing one of these three variables k_1, k_2, and b. Figs. 6 and 7 show the shapes of $\partial g/\partial k_1$ and $\partial g/\partial k_2$ for $k_1 = 1$ and separately for $k_2 = 1$. From these two plots, one may note that the shape of $\partial g/\partial k_1$ and $\partial g/\partial k_2$ are linearly independent. According to Eq. (8), the shape of Δa is a linear combination of the two surfaces in each plot. Thus, the linear independence of $\partial g/\partial k_1$ and $\partial g/\partial k_2$ ensures that we may identify the displacement of the boundary for the system with multiple simultaneous damages of small magnitude as a linear combination of the displacements of the boundaries for single damages at different locations. In addition, the stiffnesses k_1 and k_2 may be reconstructed by fitting Eq. (7) to the measured data points (a, b) in a least-squares sense.To model the possible errors in the data-collection procedure or caused by the limited resolution in varying the controlled parameter a, the values of a at nine data-points chosen on the boundary for the case of $k_1 = k_2 = 0.9$ are perturbed with random noise (normal distribution with zero mean and 0.05 standard deviation). A total of 10 000 sets of noisy data-points were generated. The mean and the standard deviation of the noisy data-points are shown in Fig. 8. Then, the stiffnesses k_1 and k_2 are reconstructed for each set. The mean of the stiffnesses k_1 and k_2 calculated are 0.8971 and 0.8972, and the corresponding standard deviations are 0.0293 and 0.0331. Compared with the exact value of the stiffness ($k_1 = k_2 = 0.9$), the reconstructed stiffnesses k_1 and k_2 based on the noisy data are very accurate, which demonstrates that the technique of fitting the bifurcation boundary to the measured data-points is robust for detecting multiple simultaneous damages. Moreover, even if the explicit expression of the bifurcation boundary (such as Eq. (7)) is not available (e.g., for a more complex system), the system parameter still can be interrogated by the same procedure based on Eq. (4) and the condition of bifurcation onset. Hence, when nonlinear feedback excitation is used for model-based identification, the accuracy of the model affects the results. Nonetheless, the proposed approach can be used also when no model is available. In such a case, however, the morphing of the bifurcation boundaries from experimental measurements are needed to reconstruct parameter variations.

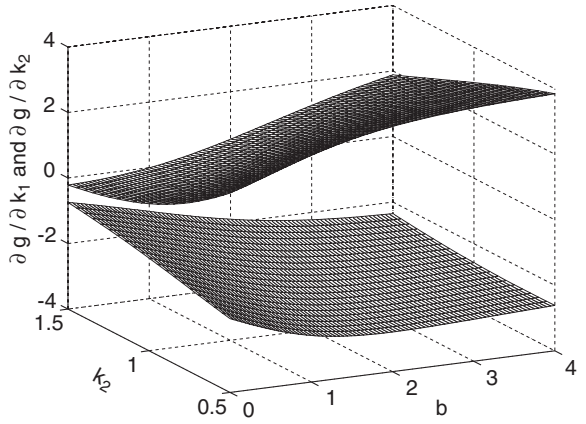

Fig. 6. The shape of the sensitivity functions $\partial g/\partial k_1$ and $\partial g/\partial k_2$ for $k_1 = 1$.

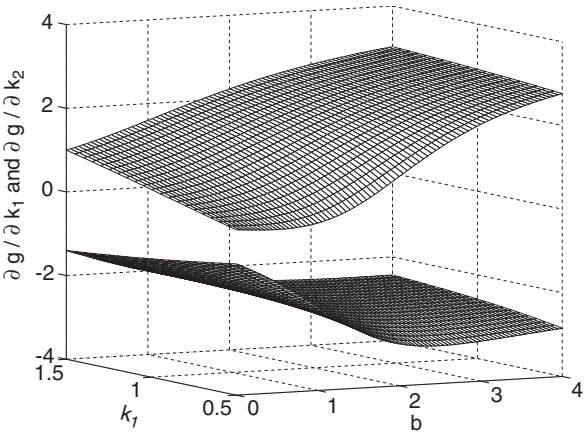

Fig. 7. The shape of the sensitivity functions $\partial g/\partial k_1$ and $\partial g/\partial k_2$ for $k_2 = 1$.

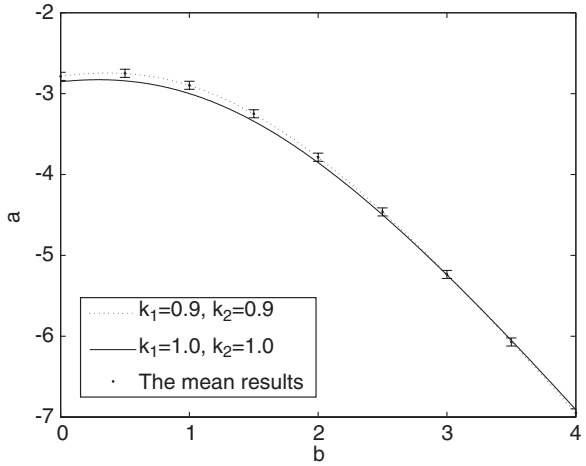

Fig. 8. Exact Hopf bifurcation boundary for the healthy system ($k_1 = k_2 = 1$) and the damaged system ($k_1 = k_2 = 0.9$), and the mean and the standard deviation of the noisy data-points generated for the damaged system.

3. Nonlinear feedback excitation

In Section 2.2, we have discussed that the linear component of the feedback excitation **GX** is designed to destabilize the system by forcing it to cross the bifurcation boundary by tuning the controlled parameters in the linear gain matrix **G**. After the bifurcation, it is desirable that the system be stable. The stabilization in the post-bifurcation regime is accomplished by the nonlinear component of the feedback excitation $\bar{\mathbf{F}}(\mathbf{X})$. As a result, nonlinear feedback excitation plays an important role in the dynamics of the system in the post-bifurcation regime. As discussed for an example of a single-degree-of-freedom oscillator in Section 2.1, the supercritical or subcritical character of the bifurcation is determined by the form of nonlinear feedback. The magnitude of the amplitude jump for subcritical bifurcations is also controlled by the parameters in the nonlinear feedback. In general, we seek the form of nonlinear feedback excitation which causes a subcritical Hopf bifurcation. There are two main reasons why a subcritical Hopf bifurcation is preferable. The first reason is that the emerging limit cycle oscillation after the bifurcation occurs provides features which are useful for detecting damage. The second reason is that the amplitude jump at the bifurcation point can facilitate the identification of the bifurcation boundary more precisely in an experimental setting. The only concern is that a large-amplitude jump may deteriorate the system. Thus, nonlinear feedback should be designed such that the amplitude of the limit cycle oscillation is as small as possible while being also large enough to accommodate the sensitivity of the measurement instrumentation. Finding the form of nonlinear feedback excitation that creates desired bifurcations may start with the understanding of the normal form of such bifurcations. In the case of two-degree-of-freedom oscillators presented in Section 2.2, first, we consider the following system which gives the canonical form for subcritical Hopf bifurcations:

$$\dot{r} = \mu r + r^3 - r^5,$$

$$\dot{\theta} = \omega, \tag{9}$$

where μ is the parameter that controls the stability of the fixed point at the origin, and ω is a constant. Suppose the states (x_1, x_2, y_1, and y_2) satisfy the relationships: $x_1 = r\cos\theta$, $x_2 = r\sin\theta$, $y_1 = \dot{x}_1$, and $y_2 = \dot{x}_2$. Then, the dynamics of the state based on Eq. (9) can be expressed as

$$\dot{x}_1 = y_1,$$

$$\dot{x}_2 = y_2,$$

$$\begin{aligned}\dot{y}_1 = {} & \mu^2 x_1 - \mu\omega x_2 - \omega y_2 + \left[4\mu(x_1^2+x_2^2) + (3-6\mu)(x_1^2+x_2^2)^2 - 8(x_1^2+x_2^2)^3 + 5(x_1^2+x_2^2)^4\right]x_1 \\ & - \omega\left[(x_1^2+x_2^2) - (x_1^2+x_2^2)^2\right]x_2,\end{aligned}$$

$$\begin{aligned}\dot{y}_2 = {} & \mu\omega x_1 + \mu^2 x_2 + \omega y_1 + \left[4\mu(x_1^2+x_2^2) + (3-6\mu)(x_1^2+x_2^2)^2 - 8(x_1^2+x_2^2)^3 + 5(x_1^2+x_2^2)^4\right]x_2 \\ & + \omega\left[(x_1^2+x_2^2) - (x_1^2+x_2^2)^2\right]x_1.\end{aligned}$$

This derivation provides insights into how one may design the simplest form of nonlinear feedback needed to cause a subcritical Hopf bifurcation. Specifically, the cubic terms are essential, as it is possible to cancel out all other higher-order terms through nonlinear coordinate transformations while maintaining topological equivalence for the state–space portrait near the bifurcation point. Therefore, in Eq. (5) in Section 2.2, $f(x_1, x_2)$ is simply assumed to be βx_2^3, where β is the controlled parameter for nonlinear feedback excitation. To demonstrate that a subcritical bifurcation can occur while such a nonlinear feedback is exploited, we choose $a = -3$ and $b = 1$ in Eq. (5) for the healthy system ($m_1 = m_2 = 1$, $k_1 = k_2 = 1$, $c_1 = c_2 = 1$). Fig. 3 shows that these chosen values for a and b are located exactly on the Hopf bifurcation boundary. Thus, the feedback excitation is designed as $\mathbf{F} = [0 \; -3x_1 + x_2 + \beta x_2^3]^{\mathrm{T}}$. The resulting equation $\dot{\mathbf{X}} = \mathbf{AX} + \mathbf{BF}$ can be expressed as

$$\begin{bmatrix}\dot{x}_1\\ \dot{x}_2\\ \dot{y}_1\\ \dot{y}_2\end{bmatrix} = \begin{bmatrix}0 & 0 & 1 & 0\\ 0 & 0 & 0 & 1\\ -2 & 1 & -2 & 1\\ 1 & -1 & 1 & -1\end{bmatrix}\begin{bmatrix}x_1\\ x_2\\ y_1\\ y_2\end{bmatrix} + \begin{bmatrix}0 & 0\\ 0 & 0\\ 1 & 0\\ 0 & 1\end{bmatrix}\begin{bmatrix}0\\ -3x_1 + x_2 + \beta x_2^3\end{bmatrix}.$$

Then, the dynamics of the system can be obtained by integrating the above system of differential equations with an adequate time marching scheme. Fig. 9 shows the stable limit cycle emerging through a Hopf bifurcation. The limit cycle is projected onto the subspace spanned by x_1 and y_1 for different values of the controlled parameter β. Fig. 9

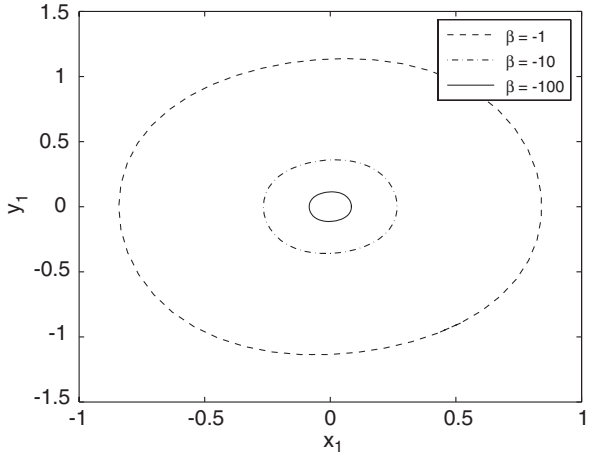

Fig. 9. The emerging stable limit cycle at the Hopf bifurcation point projected onto the subspace spanned by x_1 and y_1 for different values of the controlled parameter β.

clearly shows that the chosen form of nonlinear feedback causes a subcritical Hopf bifurcation. Also, the size of the amplitude of the limit cycle is dependent on the value of β. Thus, the appropriate amplitude jump at the bifurcation point can be designed by adjusting the value of β.

In this section, we have used an example of a two-degree-of-freedom oscillator to introduce the strategy of designing nonlinear feedback excitation to cause desired bifurcations. Next, we focus on a more complex aeroelastic system.

4. Damage detection for an aeroelastic system

The aeroelastic system considered here is composed of a nonlinear panel forced by flow-induced loads (as depicted in Fig. 10). Such a system is of interest in online damage detection in modern aircraft and the next generation of reusable launch vehicles. It has been shown that this system undergoes a variety of dynamical behaviors (Dowell, 1975, 1982). The panel may remain statically flat, buckle into a statically deformed shape, flutter with a periodic motion, or vibrate chaotically. These various dynamics of the panel depend mainly on two parameters: the magnitude of the in-plane compressive load acting on the panel, and the velocity of the fluid flow interacting with the panel. In addition to these two parameters, it is still possible for the dynamics of the panel to be qualitatively changed by actively applying a feedback excitation on the panel through the use of sensors and actuators. For example, the initially flat panel under a small in-plane compressive load and low flow velocity may be caused to flutter or buckle due to the feedback excitation. Therefore, the bifurcation boundary in parameter space spanned by the controlled parameters in the feedback excitation can be obtained by varying the controlled parameters and observing the onset of bifurcations. Finally, multiple simultaneous damages occurring in the panel may be detected by visualizing the movement and deformation of the bifurcation boundary, and by observing the post-bifurcation dynamics.

4.1. Aeroelastic model forced by feedback

The panel is considered as a nonlinear, one-dimensional, homogeneous, isotropic, and elastic thin plate with pin-supported end points. The von Karman strain–displacement relation is used to account for the structural nonlinearity resulting from the coupling of the in-plane stretching and out-of-plane deflection of the panel. The flow is modelled by piston theory (Lighthill, 1953) which provides a good approximation for the unsteady flow forces for high supersonic Mach numbers. In addition to aerodynamic loads, the panel is also excited by a feedback loop for the purpose of damage detection. Finally, a local reduction in bending stiffness in a small region around various locations along the panel is considered as a damage scenario. The governing equation for the complete aeroelastic system is obtained as follows:

$$D W'''' + \rho h \ddot{W} - Eh\eta_0 W'' - \frac{Eh}{2l}\left[\int_0^l W'^2(\xi)\,\mathrm{d}\xi\right] W'' + \frac{\rho_\infty U_\infty^2}{M}\left(W' + \frac{1}{U_\infty}\dot{W}\right) + \Delta p_s - P(X,t) = 0, \tag{10}$$

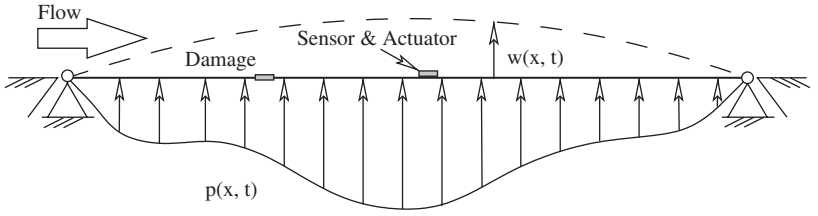

Fig. 10. Cross-section through an aeroelastic system composed of a panel subjected to unsteady supersonic flow.

where W' and $\dot{W}$ represent the spatial and time derivatives of the panel deflection W, D is a coefficient characterizing the bending stiffness of the panel ($D = Eh^3/12(1-\nu^2)$, with E being Young's modulus, and ν being Poisson's ratio). Also, ρ is the mass density of the panel, h is the panel thickness, l is the panel length, η_0 is the initial axial strain of the panel, ρ_∞ and U_∞ are the upstream far field density and velocity of the flow, M is the local Mach number, Δp_s is the static pressure difference across the plate (at zero flow velocity), and $P(X,t)$ is the transverse distributed force. The bending stiffness and Young's modulus in the damaged region of the panel are denoted by $\bar{D}$ and $\bar{E}$, and are distinct from D and E for the healthy regions.

Next, nondimensional variables x, w, and τ are defined as $x = X/l$, $w = W/h$, and $\tau = t/\sqrt{\rho h l^4/D}$, and Eq. (10) can be nondimensionalized as follows:

$$S_r w'''' + \ddot{w} - S_r R_x w'' - S_r S\left[\int_0^1 w'^2(\xi)\,\mathrm{d}\xi\right] w'' + \lambda w' + \sqrt{\frac{\mu\lambda}{M}}\dot{w} + \frac{l^4}{Dh}\Delta p_s - F(x,\tau) = 0, \tag{11}$$

where $w' = \partial w/\partial x$, $\dot{w} = \partial w/\partial \tau$, and $F(x,\tau) = l^4 P(X,t)/(Dh)$. The corresponding nondimensional coefficients in Eq. (11) are as follows: in-plane pre-load $R_x = Eh\eta_0 l^2/D$; bending–stretching coefficient $S = Eh^3/(2D) = 6(1-\nu^2)$; flow velocity $\lambda = (\rho_\infty U_\infty^2 l^3)/(MD)$; and flow mass ratio $\mu = (\rho_\infty l)/(\rho h)$. The coefficient S_r is the stiffness reduction ratio ($S_r = \bar{D}/D$) characterizing the damage level in the panel. For example, S_r equals unity when no damage is present. Also, the corresponding boundary conditions at the supports can be written in nondimensional form as

$$w''(x=0,\tau) = 0 \quad \text{and} \quad w(x=0,\tau) = 0,$$
$$w''(x=1,\tau) = 0 \quad \text{and} \quad w(x=1,\tau) = 0.$$

In this study, we consider that the panel is subjected to a small in-plane compressive load and low velocity flow such that, in the absence of the nonlinear feedback excitation, the panel is flat and stable. Because the coupling of the in-plane stretching and out-of-plane deflection of the panel is considered, the resulting structural nonlinearity corresponding to $S\left[\int_0^1 w'^2(\xi)\,\mathrm{d}\xi\right] w''$ in Eq. (11) provides a strong stabilization effect for the panel dynamics. Therefore, the feedback excitation is designed only for destabilizing the aeroelastic system so that the panel may flutter or buckle when bifurcations occur. Herein, a concentrated feedback force (in terms of transverse and angular displacements measured by a sensor) is considered to be applied to the panel through an actuator. Accordingly, the nondimensionalized feedback force $F(x,\tau)$ in Eq. (11) can be expressed as

$$F(x,\tau) = f(\tau)\delta(x - x_a) \quad \text{and} \quad f(\tau) = aw(x_s,\tau) + bw'(x_s,\tau), \tag{12}$$

where x_a and x_s are, respectively, the location of the actuator and the sensor, and a and b are the controlled parameters to be varied for identifying the bifurcation boundary.

4.2. Numerical results

The numerical approach for computing the dynamics of the aeroelastic system is to first discretize the governing partial differential equation in space by a central finite difference scheme, and then to integrate the resulting system of ordinary differential equations in time by a time marching scheme adequate for stiff systems. The computational domain is uniformly divided into m sections. All the spatial derivatives in the governing equations and the boundary conditions satisfied at the discretization points are approximated by the central finite difference formulas of second-order accuracy. Also, one ghost node is needed at each end of the panel in a central finite difference formulation. As a result, the set of ordinary differential equations for the discretized system of the panel can be expressed in state–space

matrix form as

$$\begin{bmatrix} \mathbf{I} & \mathbf{0} \\ \mathbf{0} & \mathbf{\Omega} \end{bmatrix} \begin{bmatrix} \dot{\mathbf{w}} \\ \dot{\mathbf{v}} \end{bmatrix} + \begin{bmatrix} \mathbf{0} & -\mathbf{I} \\ \mathbf{\Phi} & \mathbf{\Psi} \end{bmatrix} \begin{bmatrix} \mathbf{w} \\ \mathbf{v} \end{bmatrix} = \begin{bmatrix} \mathbf{0} \\ \mathbf{q} \end{bmatrix}, \tag{13}$$

where the vector $\mathbf{w}$ represents the displacements at all discretization points, $\mathbf{v}$ is the time derivative of $\mathbf{w}$, and $\mathbf{q}$ is the force vector corresponding to the special case of the feedback force described in Section 4.1 (i.e., $\mathbf{q} = [0, \ldots, 0, F(\tau)/\Delta x, 0, \ldots, 0]$). The matrices $\mathbf{\Omega}$, $\mathbf{\Phi}$, and $\mathbf{\Psi}$ depend on aeroelastic properties and also on $\mathbf{w}$. Hence, Eq. (13) is nonlinear. The dynamics of the panel governed by Eq. (13) was solved by using the Gear method in this study. A converged solution has been obtained for a number of sections $m = 80$ and a time step $\Delta\tau = 0.01$. In this study, a set of parameters of the aeroelastic system have been selected as $\lambda = 100$, $R_x = -\pi^2$, $v = 0.252$, and $\mu/M = 0.01$, which corresponds to the case where the panel dynamics is stable and flat. The feedback excitation designed in Eq. (12) is exploited to change the stability of the panel and force the panel to flutter with a small amplitude periodic motion in the post-bifurcation regime. Herein, we assume that the transverse and angular displacement at the middle point of the panel may be measured by a sensor, and the force from a feedback loop acts on the middle point of the panel through an actuator (i.e., x_s and x_a are both equal to $\frac{1}{2}$ in Eq. (12)).

The subcritical Hopf bifurcation boundary in the parameter space spanned by the controlled parameters a and b in Eq. (12) can be obtained by varying the value of a for fixed values of b until the onset of bifurcation is observed. As demonstrated in Fig. 11, at the bifurcation point ($a = -468.7$ and $b = 0$), the projection of the emerging dynamics of

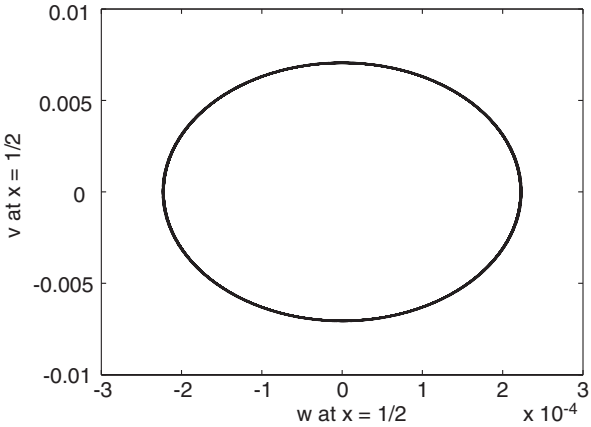

Fig. 11. The limit cycle projected onto the subspace spanned by the displacement and the velocity at the middle point of the healthy panel ($x = \frac{1}{2}$) at the bifurcation point ($a = -468.7$ and $b = 0$).

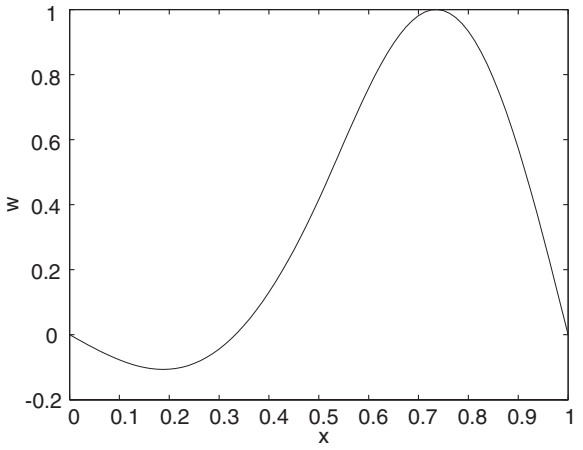

Fig. 12. The first dominant mode present in the dynamics of the panel when a bifurcation occurs ($a = -468.7$ and $b = 0$).

the healthy panel onto the subspace spanned by the displacement and the velocity at the middle point of the panel ($x = \frac{1}{2}$) is a limit cycle with a small amplitude, which shows that the designed feedback successfully induces a subcritical Hopf bifurcation causing the panel to flutter. Also, by analyzing the snapshots of the panel flutter based on proper orthogonal decomposition (Epureanu et al., 2004a, b; Azeez and Vakakis, 2000), we conclude that there is only one dominant mode present in the dynamics of the panel, as shown in Fig. 12. Furthermore, this dominant mode is nearly identical to the eigenmode corresponding to the pair of eigenvalues (of the Jacobian matrix of Eq. (13) at the equilibrium state of the panel) located exactly on the imaginary axis of the complex plane at the bifurcation point ($a = -468.7$ and $b = 0$). Therefore, the dominant frequency and the dominant mode shape of the panel dynamics at the bifurcation point are related to the form of the linear component of the feedback and the controlled parameters.

Next, several damage scenarios are considered to investigate the sensitivity of the proposed approach to the variation in structural parameters used to model the damage, and to demonstrate its effectiveness in detecting multiple simultaneous damages. The damage scenarios include different levels (10% and 20%) of bending stiffness loss of the panel expanding along 1.25% of panel length around different locations (at the quarter point $x = \frac{1}{4}$ and at the middle point $x = \frac{1}{2}$). Fig. 13 shows that Hopf bifurcation boundaries for the panels with damage around $x = \frac{1}{2}$ move monotonically and proportionally away from the boundary for the healthy panel when the damage level increases. In Fig. 14, one may note that the boundaries for the panel with damage around $x = \frac{1}{4}$ and the healthy panel are not

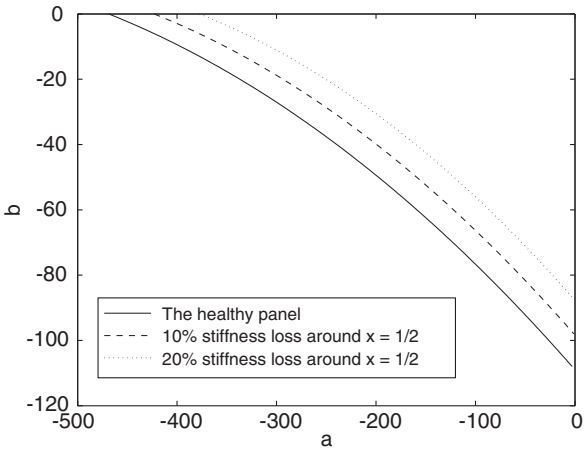

Fig. 13. Hopf bifurcation boundaries for the healthy panel and damaged panels with different levels of damage.

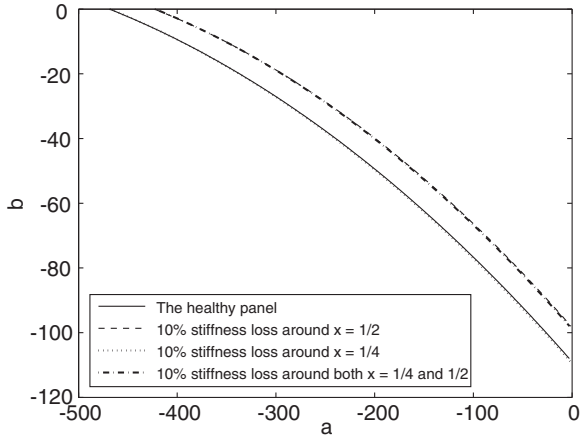

Fig. 14. Hopf bifurcation boundaries for the healthy panel and damaged panels with different locations of damage.

distinguishable, and so are the boundaries for the panels with damage around $x = \frac{1}{2}$ and with multiple damages both around $x = \frac{1}{2}$ and $\frac{1}{4}$. These results show that the bifurcation boundary due to the specific designed feedback (where x_s and x_a are both equal to $\frac{1}{2}$ in Eq. (12)) is not sensitive to damage occurring around $x = \frac{1}{4}$. Hence, multiple simultaneous damages around $x = \frac{1}{2}$ and $\frac{1}{4}$ are difficult to detect because the movement of the boundary for the system with multiple simultaneous damages with respect to the boundary for the healthy system is a linear combination of the movements of the boundaries for the systems with single damages at different locations (as discussed in Section 2.2). Nevertheless, in addition to the observation of the movement of the bifurcation boundary, the resulting dynamical features of the panel along the bifurcation boundary may also be utilized to detect damage. These features include the dominant frequency, the shape of the dominant mode, and the maximum amplitude of the panel flutter. The dominant frequency and the corresponding mode shape are related to the eigenanalysis of the Jacobian matrix when the system loses stability due to the linear feedback. Thus, the sensitivities of these two features to parametric variation are similar to ones for the bifurcation boundary, and are small for some cases, as shown in Fig. 14. In contrast, the amplitude of the flutter is mainly controlled by the structural nonlinearity and has high sensitivity to parametric variation. Fig. 15 shows the maximum displacement amplitude of the emerging panel flutter (limit cycle oscillation) at $x = \frac{1}{2}$ along the bifurcation boundaries corresponding to different values of b for the healthy panel

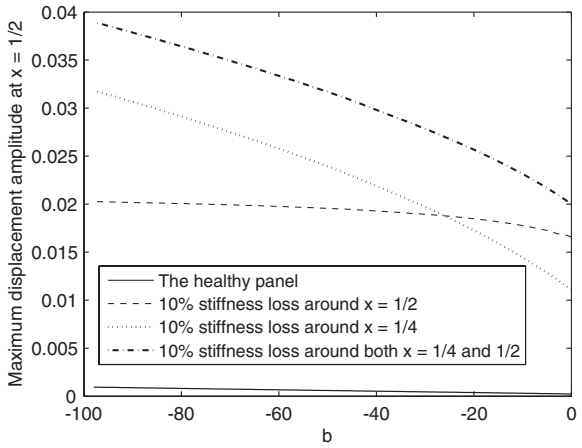

Fig. 15. The maximum displacement amplitude of the emerging panel flutter (limit cycle oscillation) at $x = \frac{1}{2}$ along the bifurcation boundaries corresponding to different values of b for the healthy panel and the different damaged panels shown in Fig. 14.

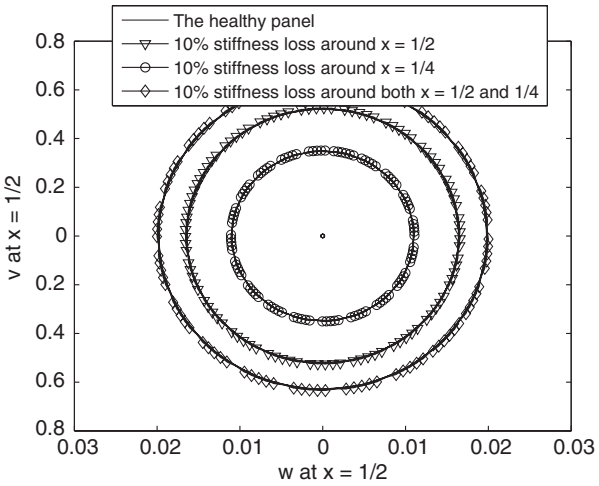

Fig. 16. The limit cycle projected onto the subspace spanned by the displacement and the velocity at $x = \frac{1}{2}$ for the healthy panel and the different damaged panels at the bifurcation point corresponding to $b = 0$ in Fig. 15.

and different damaged panels. Also, Fig. 16 shows the limit cycles projected onto the subspace spanned by the displacement and velocity at $x = \frac{1}{2}$ for the healthy panel and the different damaged panels at the bifurcation point (corresponding to $b = 0$ in Fig. 15). From these two figures, one may note that the flutter amplitude for the various damaged panels changes dramatically and very differently from the healthy panel dynamics, which means that a single damage at different locations of the panel or multiple simultaneous damages in the panel may be detected based on the flutter amplitude at the bifurcation point. Fig. 15 also reveals that nonlinearity plays an important role in enhancing sensitivity for damage detection.

Finally, we present a quantitative comparison of sensitivity of the proposed approach for damage detection with a common linear method based on the modal frequencies as its features. Herein, the damage in the panel is considered as 10% loss of the bending stiffness of the panel expanding along 1.25% of panel length around the middle point $x = \frac{1}{2}$ of the panel. The relative difference in the first modal frequency between the damaged panel and the healthy panel is 0.15%. In contrast, the relative difference in the controlled parameter a at the Hopf bifurcation point (where $b = 0$) between the damaged panel and the healthy panel is 9.7%, which shows that sensitivity is highly increased.

The lack of sensitivity in detecting the damage around the quarter point $x = \frac{1}{4}$ of the panel leads to difficulties in the parameter reconstruction technique demonstrated in Section 2.2. Nevertheless, these difficulties are alleviated by observing the resulting dynamical features of the panel in the post-bifurcation regime.

5. Conclusions and discussion

In this article, the key idea of a novel proposed damage detection approach has been discussed by exploring a single-degree-of-freedom oscillator forced by a nonlinear feedback. The detailed methodology has been formulated and then demonstrated for an example of a two-degree-of-freedom mass–spring–damper system. In addition, the strategy of designing nonlinear feedback excitation that causes desired bifurcations has also been addressed. Finally, a more complex and practical example as a nonlinear panel interacting with an unsteady supersonic flow has been investigated. Damage has been modelled as a loss of stiffness in a portion of the plate. The results presented in these examples have shown that the proposed damage detection approach provides high sensitivity and high robustness, and may be exploited to detect multiple simultaneous damages. Nonetheless, the energy required by the proposed approach to be injected in the system for interrogation can be higher than other approaches, depending on the particular application. For some applications, this energy (and the resulting stresses) can be large, as would be the case for several civil structures for example. However, aerospace applications that the proposed approach is envisioned for have considerably distinct features. For example, wings occasionally operate in regimes that are close to the stability boundaries, or even go beyond these limits such as in the case of wings exhibiting limit cycle oscillations during operation. In these cases, the energy (and stress) required to interrogate the system using the proposed approach is not high (and may be harvested through the manipulation of the operational loads). Hence, the level of energy injection is similar to other (global) vibration-based techniques based on modal properties. Nonetheless, there are also other techniques that use considerably lower energy, such as is the case of detection using ultrasound, but these are local approaches and typically require a larger number of sensors or have other limitations.

The detection of the bifurcation point can be difficult for many systems exhibiting supercritical-type bifurcations, where there is no clear jump from a small amplitude solution to a large amplitude solution. The use of subcritical bifurcations alleviates this problem, as subcritical bifurcations are typically sharp, so that the bifurcation point is well defined and reproducible (while also allowing for the estimation of the detection error).

A related matter is the case where g is not known analytically. Then the approach presented herein can be used not as a model-based approach, but as a model-less approach. Of course, since a model is not available, more measurements are required. Specifically, the bifurcation boundary is measured and its morphing is determined (experimentally) for various system parameters that are of interest. Next, the morphing of the boundary is used for damage detection as shown in Section 4.2 for an aeroelastic system.

Symmetry breaking is a factor that affects most real systems. Surely, a supercritical bifurcation point is affected significantly by symmetry breaking. To account for that, the approach herein is most advantageous if designed to monitor (as a feature) the jump at the appearance/disappearance of the large amplitude solution. That solution is not topologically affected by symmetry breaking, and hence, the bifurcation morphing approach is marginally affected, especially for model-less applications. These issues are most effectively estimated in experimental results which are beyond the scope of this paper, and are the focus of ongoing and future work.

Acknowledgements

The authors wish to acknowledge the National Science Foundation (CAREER program) and Professor Masayoshi Tomizuka and Dr Shih-Chi Liu (program directors) for the generous support of this work.

References

Abdalla, M.O., Grigoriadis, K.M., Zimmerman, D.C., 1998. Enhanced structural damage detection using alternating projection methods. AIAA Journal 36 (7), 1305–1311.

Amaravadi, V.K., Mitchell, K., Rao, V.S., Derriso, M.M., 2002. Structural integrity monitoring of composite patch repairs using wavelet analysis and neural networks. In: Davies, L.P. (Ed.), Proceedings of SPIE: Smart Structures and Materials 2002: Smart Structures and Integrated Systems, vol. 4701, San Diego, California, pp. 156–166.

Amizic, B., Amaravadi, V.K., Rao, V.S., Derriso, M.M., 2002. Two-dimensional wavelet mapping techniques for damage detection in structural systems. In: Rao, V.S. (Ed.), Proceedings of SPIE: Smart Structures and Materials 2002: Modeling, Signal Processing, and Control, vol. 4693, San Diego, California, pp. 267–278.

Azeez, M.F.A., Vakakis, A.F., 2000. Proper orthogonal decomposition of a class of vibroimpact oscillations. Journal of Sound and Vibration 240 (5), 859–889.

Cao, T.T., Zimmerman, D.C., 1999. Procedure to extract Ritz vectors from dynamic testing data. Journal of Structural Engineering 125 (12), 1393–1400.

Chancellor, R.S., Alexander, R.M., Noah, S.T., 1996. Detecting parameter changes using experimental nonlinear dynamics and chaos. ASME Journal of Vibration and Acoustics 118 (3), 375–383.

Chatterjee, A., Cusumano, J.P., Chelidze, D., 2002. Optimal tracking of parameter drift in a chaotic system: experiment and theory. Journal of Sound and Vibration 250 (5), 877–901.

Chelidze, D., Cusumano, J.P., 2004. A dynamical systems approach to failure prognosis. ASME Journal of Vibration and Acoustics 126 (1), 2–8.

Chelidze, D., Cusumano, J.P., Chatterjee, A., 2002. A dynamical systems approach to damage evolution tracking, Part 1: description and experimental application. ASME Journal of Vibration and Acoustics 124 (2), 250–257.

Cusumano, J.P., Chelidze, D., Chatterjee, A., 2002. A dynamical systems approach to damage evolution tracking, Part 2: model-based validation and physical interpretation. ASME Journal of Vibration and Acoustics 124 (2), 258–264.

Doebling, S.W., Farrar, C.R., Prime, M.B., Shevitz, D.W., 1996. Damage identification and health monitoring of structural and mechanical systems from changes in their vibration characteristics: a literature review. Report LA-13070-MS, Los Alamos National Laboratories, Los Alamos, NM.

Dowell, E.H., 1975. Aeroelasticity of Plates and Shells. Noordhoff International Publishing, Leyden.

Dowell, E.H., 1982. Flutter of a buckled plate as an example of chaotic motion of a deterministic autonomous system. Journal of Sound and Vibration 85 (3), 333–344.

D'Souza, K., Epureanu, B.I., 2005a. Damage detection in nonlinear systems using system augmentation and generalized minimum rank perturbation theory. Smart Materials and Structures, to appear.

D'Souza, K., Epureanu, B.I., 2005b. System augmentation and matrix updating for damage detection in nonlinear systems. In: Proceedings of the 46th AIAA/ASME/ASCE/AHS/ASC Structures, Structural Dynamics and Materials Conference, vol. AIAA-2005-1831, Austin, Texas.

Epureanu, B.I., Yin, S.H., 2004. Identification of damage in an aeroelastic system based on attractor deformations. Computers and Structures 82 (31–32), 2743–2751.

Epureanu, B.I., Tang, L.S., Païdoussis, M.P., 2004a. Coherent structures and their influence on the dynamics of aeroelastic panels. International Journal of Non-linear Mechanics 36 (9), 977–991.

Epureanu, B.I., Tang, L.S., Païdoussis, M.P., 2004b. Exploiting chaotic dynamics for detecting parametric variations in aeroelastic systems. AIAA Journal 42 (4), 728–735.

Epureanu, B.I., Yin, S.H., Derriso, M.M., 2004c. Attractor-based damage detection in a plate subjected to supersonic flows. In: Proceedings of SPIE Ninth International Symposium on NDE for Health Monitoring and Diagnostics, vol. 5394, San Diego, California, pp. 340–350.

Epureanu, B.I., Yin, S.H., Derriso, M.D., 2005a. High-sensitivity damage detection based on enhanced nonlinear dynamics. Smart Materials and Structures 14 (2), 321–327.

Epureanu, B.I., Yin, S.H., Dowell, E.H., 2005b. Enhanced nonlinear dynamics for accurate identification of stiffness loss in a thermo-shielding panel. Nonlinear Dynamics 39 (1–2), 197–211.

Farrar, C.R., Doebling, S.W., Nix, D.A., 2001. Vibration-based structural damage identification. Philosophical Transactions of the Royal Society of London: a—Mathematical, Physical and Engineering Sciences 359 (1778), 131–149.

Koh, B.H., Ray, L.R., 2003. Localisation of damage in smart structures through sensitivity enhancing feedback control. Mechanical Systems and Signal Processing 17 (4), 837–855.

Lighthill, M.J., 1953. Oscillating airfoils at high Mach number. Journal of the Aeronautical Sciences 20 (6), 402–406.

Loh, C.H., Tou, I.C., 1995. A system identification approach to the detection of changes in both linear and nonlinear structural parameters. Earthquake Engineering and Structural Dynamics 24 (1), 85–97.

Nichols, J.M., Todd, M.D., Seaver, M., Virgin, L.N., 2003a. Use of chaotic excitation and attractor property analysis in structural health monitoring. Physical Review E 67 (016209), 1–8.

Nichols, J.M., Todd, M.D., White, J.R., 2003b. Using state–space predictive modeling with chaotic interrogation in detecting joint preload loss in a frame structure experiment. Smart Materials and Structures 12 (2), 580–601.

Nichols, J.M., Trickey, S.T., Todd, M.D., Virgin, L.N., 2003c. Structural health monitoring through chaotic interrogation. Meccanica 38 (2), 239–250.

Nichols, J.M., Virgin, L.N., Todd, M.D., Nichols, J.D., 2003d. On the use of attractor dimension as a feature in structural health monitoring. Mechanical Systems and Signal Processing 17 (6), 1305–1320.

Pappa, R.P., James, G.H., Zimmerman, D.C., 1998. Autonomous modal identification of the space shuttle tail rudder. Journal of Spacecraft and Rockets 35 (2), 163–169.

Ray, L.R., Koh, B.H., 2003. Enhancing uniqueness properties in damage identification using sensitivity enhancing control. Materials Evaluation 61 (10), 1134–1142.

Ray, L.R., Tian, L., 1999. Damage detection in smart structures through sensitivity enhancing feedback control. Journal of Sound and Vibration 227 (5), 987–1002.

Smyth, A.W., Masri, S.F., Caughey, T.K., Hunter, N.F., 2000. Surveillance of mechanical systems on the basis of vibration signature analysis. Journal of Applied Mechanics 67 (3), 540–551.

Sohn, H., Farrar, C.R., 2001. Damage diagnosis using time series analysis of vibration signals. Smart Materials and Structures 10 (3), 446–451.

Todd, M.D., Nichols, J.M., Pecora, L.M., Virgin, L.N., 2001. Vibration-based damage assessment utilizing state–space geometry changes: local attractor variance ratio. Smart Materials and Structures 10 (5), 1000–1008.

Trendafilova, I., 2003a. A state–space based approach to health monitoring of vibrating structures. Materials Science Forum 440 (4), 203–210.

Trendafilova, I., 2003b. State–space modelling and representation for vibration-based damaged assessment. Key Engineering Materials 245 (2), 547–555.

Trickey, S.T., Todd, M., Seaver, M., Nichols, J., 2002. Geometric time domain methods of vibration based damage detection. In: Proceedings of the SPIE Ninth Smart Structures and Materials Conference, vol. 1. San Diego, California, pp. 1–9.

Wang, W.J., Wu, Z.T., Chen, J., 2001. Fault identification in rotating machinery using the correlation dimension and bispectra. Nonlinear Dynamics 25 (4), 383–393.

Zimmerman, D.C., 1999. Looking into the crystal ball: the continued need for multiple viewpoints in damage detection. Key Engineering Materials: Damage Assessment of Structures 167–168 (1), 76–90.

Zimmerman, D.C., 2000. Model validation and verification of large and complex space structures. Inverse Problems in Engineering 8 (2), 93–118.